Moment resisting on-site splice of large glulam elements by use of mechanically coupled long threaded rods

Martin Cepelka[1*], Kjell Arne Malo[1**]

[1] Department of Structural Engineering, Norwegian University of Science and Technology (NTNU), Rich. Birkelandsvei 1A, 7491, Trondheim, Norway

[*] corresponding author, martin.cepelka@ntnu.no, +4795409031

[**] kjell.malo@ntnu.no

Abstract

Large spans of modern timber bridges can be achieved by use of glulam arches with network hanger configuration. Since transportation and production limit the length of timber elements, the glulam arches must be spliced on bridge site. However, it is difficult to obtain practical moment resisting on-site splicing of massive glulam elements featuring flexural rigidity by the available timber splicing techniques. Consequently, the arches are often designed as trusses containing a large number of connections, which are costly and present a risk of decay development. In the present paper, a novel splicing technique suitable for large massive timber sections is presented. The flexural rigidity of the joint is obtained by the utilisation of long threaded rods having large withdrawal stiffness. Fast and easy on-site assembly is facilitated by mechanical coupling of the rods. The rods are oriented with a small inclination to grain, which prevents potential development of shrinkage cracks along the rods. Experimental and numerical methods were used to investigate the flexural joint characteristics. The joint prototypes featured large rotational stiffness without initial slip. As a basis for practical joint design, analytical relations are proposed for estimating the rotational stiffness, the moment capacity and the capacity under combined bending and normal force.

Keywords: long threaded rod, timber splice joint, glulam, 3D finite element model, rotational stiffness, moment capacity

1. Introduction

Feasibility studies of glulam arch bridges with network hanger configuration have shown excellent structural properties for bridges with massive glulam arches spanning up to 100-120 m [1, 2]. Since the timber arches cannot be produced and transported in one piece, the timber elements must be spliced on bridge site. In order to maintain the stability of the arches, it is crucial to incorporate flexural rigidity in the splice connections [3-5].

Figure 1 shows the recently erected network arch bridge Steibrua in Norway [6]. With a span of 88 m, the bridge is currently the longest single-span timber road bridge in the world. However, due to the lack of rotationally stiff splicing solution for large timber elements, the arches of Steibrua are formed as hybrid timber-steel trusses. This is probably not the most optimal solution since the trusses contain a large number of connections, which are expensive and vulnerable to decay developments. A more durable and cheaper solution could be achieved by the use of massive glulam arches, necessitating on-site splice joints with sufficient rotational stiffness.

Figure 1: Steibrua, Norway – Network arch bridge with glulam arches [6].

The pros and cons of different splice connection techniques in timber engineering are discussed in [7]. Recent research on steel rods glued into timber has demonstrated that connections featuring large stiffness and capacity can be achieved by using high strength epoxy adhesives [8-11]. However, for large joints, multiple rods are necessary, and the brittleness of the adhesives can lead to a progressive failure in a group of rods [12]. Therefore, design provisions for ductile failure are necessary [13-17]. The main shortcoming associated with the application of glued-in rods is the production. Experience from reviewers of failed joints revealed inadequately mixed and incorrectly applied epoxy on site. Nowadays, the production is limited to a climate controlled environment with quality control and skilled personnel [12].

The difficulties connected to gluing of rods are avoided by using long threaded rods, which are simply driven into pre-drilled holes in timber. Large rotational stiffness and moment capacity of spliced timber beams was achieved in [18] by using commonly available long threaded rods (SFS WB-T-20). The rods were inserted parallel to the grain in the opposed parts of timber beams, and the mutual splicing of the rods was carried out by grout-filled steel couplers (similar to systems used for reinforced pre-cast concrete). The parallel to grain orientation of the threaded rods enables effective force transfer in the axial direction and allows the utilisation of the high withdrawal stiffness of rods parallel to the grain. On the other hand, the development of shrinkage cracks (in the grain direction) in close proximity to the threaded rods can lead to loss of capacity. In addition, the gluing operation on site implies quality control issues, and curing of the glue affects the final setting time of the joint.

In this paper, a novel splicing solution is presented, which overcomes the aforementioned shortcomings by the use of slightly inclined long threaded rods with a metric threaded part at one end. A principle layout of the joint is shown in Figure 2. Inserting the rods with a small inclination to the grain avoids the risk of failure due to the occurrence of shrinkage cracks since the rods cross several “layers” of wood. The mechanical joint of the rods allows easy and fast on-site mounting without the need of special tools. In order to transmit the normal force acting in the arch, mutual contact of the mating timber end faces is assured by tightening the rods in the couplers. The shear force can be transmitted through shear keys. A reliable prediction of the structural properties and ductile behaviour is achieved by design provisions enforcing a failure mode driven by yielding of the steel rods.

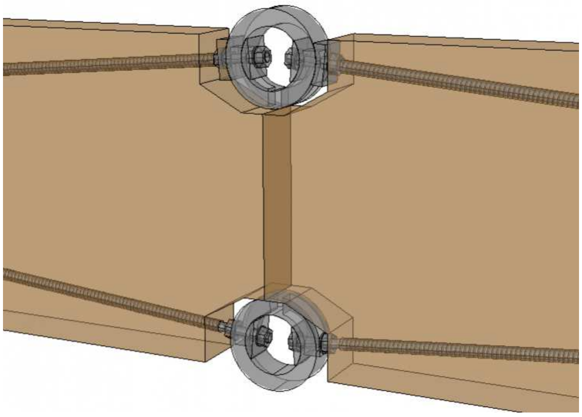

Figure 2: Principle layout of the splice joint with inclined mechanically coupled long threaded rods.

The key prerequisite regarding splicing of massive glulam arches is a sufficient and predictable rotational stiffness of the splice joints. Therefore, the main objective of the present work is to determine the flexural characteristics of the proposed splicing technique by the use of experimental testing on full-scale prototype joints and numerical models. In order to allow for practical design of the joint, analytical relations are here proposed for the determination of the rotational stiffness, the moment capacity and the combined capacity for bending moment and normal force.

2. Materials and methods

2.1. Analytical prediction of flexural joint characteristics

2.1.1. Rotational stiffness

An analytical model for the determination of the rotational stiffness of a splice joint using long threaded rods inserted parallel to the grain was derived in [18]. However, due to the inclination of the rods in the proposed splicing solution, a lateral force component is present at the rod-ends. A modification of the model accounting for the lateral deformations of the rods is presented in the following, with input parameters specified in the Appendix. The model parameters are shown in Figure 3. Here, h and b are the height and the width of the cross-section respectively, a_0 is the height of wood in compression, a_i is a coordinate along z-axis of the i-th rod row determined from the upper edge of wood in compression (with reference to Figure 3, a_i is negative for the rods in compression), h_t is the height of timber end faces in mutual contact, θ represents the relative rotation of the end timber faces, γ is the rod-to-grain angle, σ_x is the longitudinal compression stress in wood, K_{si} is the stiffness of the i-th rod row, u_i is the horizontal displacement at the i-th rod row, $z_i = a_i - a_0$ is the z-coordinate of the the i-th rod row, and F_i is the force in the i-th rod row found by [18]:

$$F_i = K_{si} \cdot u_i = K_{si} \cdot \theta \cdot z_i \, .$$

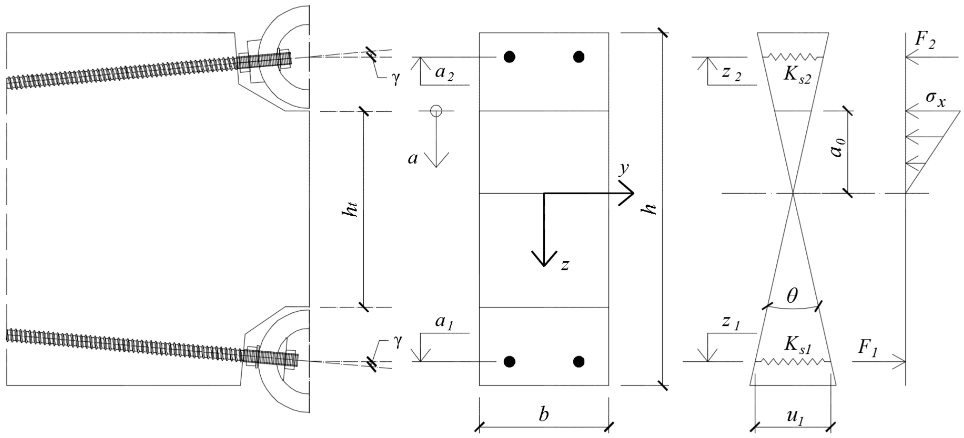

Figure 3: Analytical model nomenclature.

The analytical model presented in [18] is based on the assumption that the relative rotation of the end faces of the splice connection caused by the action of bending moment is approximated by a relative rotation of the end sections of a beam portion of length $2l_c$. The flexural stiffness is thus governed by the deformation of the wooden part in compression and the elongation and the contraction of springs representing the axial stiffness of the steel rods.

The position of the neutral axis is obtained by requiring no resulting axial force [18]:

$$a_0 = \frac{-\sum_{i=1}^{n} K_{si} + \sqrt{\left(\sum_{i=1}^{n} K_{si}\right)^2 + \frac{E \cdot b}{l_c} \cdot \sum_{i=1}^{n} K_{si} \cdot a_i}}{\frac{E \cdot b}{2 \cdot l_c}} \qquad (1)$$

where E is the elastic modulus of timber parallel to the grain, l_c represents an equivalent length of the compression (crushing) zone at the mutual contact of the wooden parts (l_c is assumed to be of equal size on both sides of the contact interface of the timber parts), and n is the number of the rod rows. The rotational stiffness of the connection k_θ is determined by [18]:

$$k_\theta = \sum_{i=1}^{n} K_{si} \cdot z_i^2 + \frac{E \cdot b \cdot a_0^3}{6 \cdot l_c} \tag{2}$$

More information and expressions for the determination of K_{si} and l_c are given in the Appendix.

2.1.2. Moment capacity

The moment capacity of the splice joint, M_u, is estimated under the assumption of elastic distribution of forces until an ultimate force is reached in either of the rods or in the timber (bilinear approximation) by:

$$M_u = \min \begin{Bmatrix} F_{u,i} \cdot z_{eq,i} \\ M_{u,t} \end{Bmatrix} \tag{3}$$

where $M_{u,t}$ is the moment capacity corresponding to the compression strength of timber, $F_{u,i}$ is the ultimate force in the i-th rod row and $z_{eq,i}$ is the equivalent lever arm of the i-th rod row given by:

$$z_{eq,i} = \frac{M}{F_i} = \frac{k_\theta}{K_{si} \cdot z_i} \tag{4}$$

The moment capacity corresponding to the compression strength of timber $M_{u,t}$ (with a linear distribution of compression stresses as illustrated in Figure 3) is determined by:

$$M_{u,t} = \frac{2 \cdot k_\theta \cdot l_c \cdot f_{c,0}}{E \cdot a_0} \tag{5}$$

where $f_{c,0}$ is the timber strength in compression parallel to the grain.

The ultimate force in the i-th rod row, $F_{u,i}$, is obtained by:

$$F_{u,i} = n_r \cdot \cos\gamma \cdot \min\left(R_{axu}, R_u\right) \tag{6}$$

where n_r is the number of the rods in one row, R_{axu} is the ultimate withdrawal strength of the rods and R_u is the tensile strength of the rods. See the Appendix for more details and determination of R_{axu}.

2.1.3. Capacity under combined action of bending moment and normal force

The interaction of bending moment and normal force acting in the splice joint was studied by the use of numerical models. It is proposed to verify the joint capacity by a modification of the relation provided by Eurocode 5 [19] for combined bending and axial compression:

$$\left(\frac{N}{N_u}\right)^2 + \frac{M}{M_u} \leq 1 \tag{7}$$

where N and M are the normal force and the bending moment acting in the joint, respectively, and N_u and M_u are the capacity in axial compression and bending, respectively.

The ultimate normal force, N_u, is determined assuming a ductile post-elastic behaviour in both the rods and the timber in compression by:

$$N_u = \sum_{i=1}^{n} F_{u,i} + b \cdot h_t \cdot f_{c,y} \tag{8}$$

where $f_{c,y}$ is the asymptotic final compression stress in timber, which is assumed as 0.8 $f_{c,0}$ [20]. The asymptotic compression stress $f_{c,y}$ corresponds to a simplified bilinear elastic plastic stress-strain curve for timber in compression parallel to the grain according to [21], as illustrated in Figure 4.

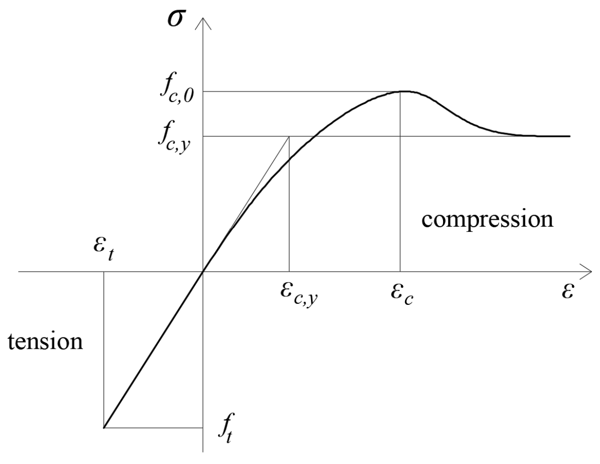

Figure 4: Stress-strain relation for timber in axial tension and compression parallel to the grain [21]

Note that due to different failure modes, the moment capacity by Eq. (5), is based on a linear elastic stress distribution in timber, while the compression capacity by Eq. (8) is based on a ductile "plastic" stress distribution. It was observed in [18] that an increasing rotation in the joint gives rise to shear stresses and tensile stresses perpendicular to the grain in the compression zone, due to change of slope at the rotated end faces. The possible "plastification" of the compression zone is thus accompanied by occurrence of cracks along the grain near the neutral axis, which limit the bending capacity. On the contrary, the failure mode in timber in pure compression is quite ductile [20].

2.2. Experimental tests

2.2.1. Experimental set-up

The prototype beam splices were tested in a four-point bending configuration yielding a pure bending in the splice connection. The experimental set-up and the detailing of the joint are shown in Figure 5 and Figure 7, respectively. The relative rotations of the end faces (denoted θ in Figure 3) were obtained by linear regression of the horizontal displacements, monitored by the digital image correlation (DIC) system ARAMIS [22] along vertical sections placed at both spliced beams in a distance of 130 mm from the axis of symmetry of the joint (this corresponds to a distance of approximately 10-20 mm from the outmost edge of the slots for the rod couplers). The measurements by DIC were validated by use of additionally applied transducers. The transducers were located on one side of the beam (confer Figure 6), and the other side of the beam was monitored by DIC. In total, two rotational transducers (denoted as T1 and T2 in Figure 6) and five displacement transducers (denoted as T3 - T7) were placed across the end faces of the splice joint. Linear approximation between the relative displacements obtained from the displacement transducers at the compression and the tension side, respectively, was used to determine the relative rotations of the end faces. The load was applied according to the loading procedure given in EN 26891:1991 [23].

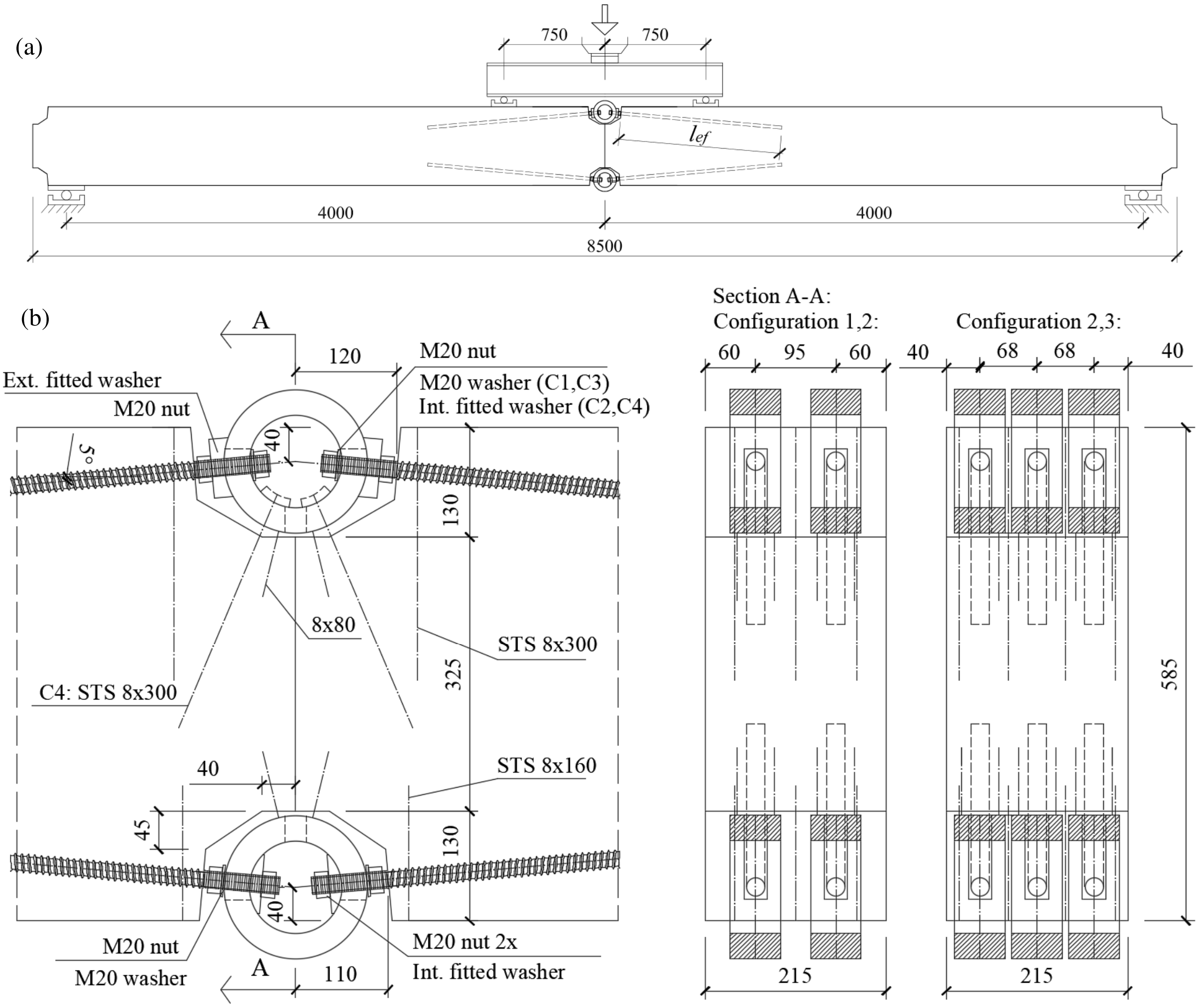

Figure 5: Experimental set-up: (a) the spliced beam, (b) technical specification of the joint. Measures given in mm.

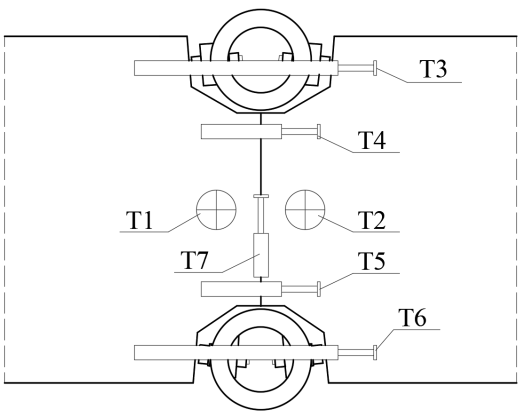

Figure 6: Schematic visualization of transducer locations.

The experimental programme is summarised in Table 1. The purpose of the experiments was to investigate the structural performance for different geometrical configurations, making available validation cases for numerical studies. Therefore, one test for each configuration was performed. Four geometrical configurations were tested, in which number of rods, effective length of rods, l_{ef} (the length of rod screwed in the timber), and detailing in the rod couplers were varied. The threaded rods, inserted in the opposed parts of the beams with a constant rod-to-grain angle of 5 degrees, were connected in the rod couplers. Purpose-made fitted washers were used to distribute the force from the rods onto the surface of the couplers. The detailing at the compression couplers was varied in the different configurations. The configurations C1 and C3 contained, besides the external fitted washers, standard M20 washers at the inner side (see Figure 7c), while in C2 and C4, the fitted internal washers were used (see Figure 7d and Figure 7e). The timber end faces of the spliced parts of the beams were brought in direct mutual contact provided by tightening the nuts. It should be noted that the level of pre-stress at the end grains is difficult to quantify due to unequal planeness of the surfaces. The nuts were tightened until the end faces were in a full mutual contact with no clearances. Since no initial slip was observed in any of the tested specimens, this procedure seems to provide a sufficient contact of the end faces.

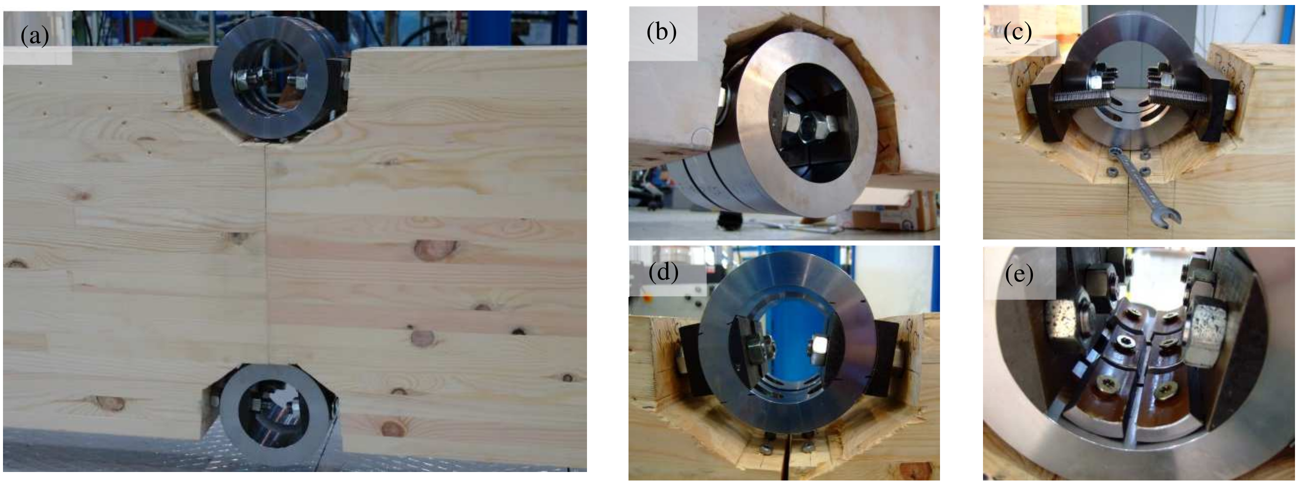

Figure 7: Detailing of the joint: (a) the assembled joint (C1), (b) detail at the tension side (C3). Details at the compression side: (c) C3 under assembly, (d) C2 after testing, (e) C4.

Table 1: Experimental programme

Config.	n_r	l_{ef} [mm]	DA1	DA2	Notation
C1	2	1850	no	no	C1-2-1850-0-0
C2	2	1200	yes	no	C2-2-1200-1-0
C3	3	1200	no	no	C3-3-1200-0-0
C4	3	1000	yes	yes	C4-3-1000-1-1

Design Alternative:

DA1 - Application of internal fitted washers in compression couplers

DA2 - Anchorage of compression couplers

Lateral displacements of the prototype rod couplers at the tension side were prevented by the use of screws inserted in pairs underneath the couplers at each side of the connection. The compression rod couplers were anchored to the timber by self-tapping screws in C4 (see Figure 7e). Perpendicular-to-grain reinforcement was applied by the use of self-tapping screws (STS). Three STS were used in the C1 and C2 configurations, while in the C3 and C4, four STS were used at each side of the timber beams.

2.2.2. Dimensions and materials

The timber beams were made of glulam strength class GL30c [24] and had 215 mm width and 585 mm height. The beams were fabricated with 33 mm thick lamellas of Scots pine. The timber specimens were conditioned at the standard environment of 20º C and 65 % relative humidity, resulting in approximately 12 % moisture content.

The purpose-made threaded rods allow fast mounting using rod couplers. The geometry of the rods is shown in Figure 8, and the average outer and inner diameters were d = 22.4 mm and d_1 = 16.9 mm, respectively. The initial 90 mm long part of the rods was manufactured with an M20 metric threaded part. The declared strength class is 8.8. In order to verify the strength of the rods, three tensile tests of the rods were carried out. The obtained mean capacity was 207.6 kN (COV = 0.01), which corresponds to a mean strength of 925 MPa if the average inner diameter is assumed.

Figure 8: Purpose-made long threaded rods used in the investigation (left) and geometry of the wood thread (right). Measures given in mm.

The rod couplers were manufactured from steel S355. The outer and inner diameters were 170 mm and 110 mm, respectively, and the width was 60 mm. The 28 mm wide slot in the couplers allowed the application of the couplers after the timber parts were brought together. It should be noted that the couplers were generally-suited prototypes designed for the purpose of the experimental investigation. The fitted washers were made of steel S355 and had a width of 60 mm and a height of 70 mm. The thickness was 15 mm at the axis of symmetry.

2.3. Numerical model

Numerical simulations were carried out by ABAQUS [25]. The geometrical layout of the numerical model corresponds to the experimental investigation shown in Figure 7. The splice joint details of the model are shown in Figure 9. Given the symmetry of the problem, only half of the beam was modelled. Transverse displacements of the beam and the rod couplers were prevented. Loading was applied through a displacement rate at the top of the beam, corresponding to the experiments (4-point bending).

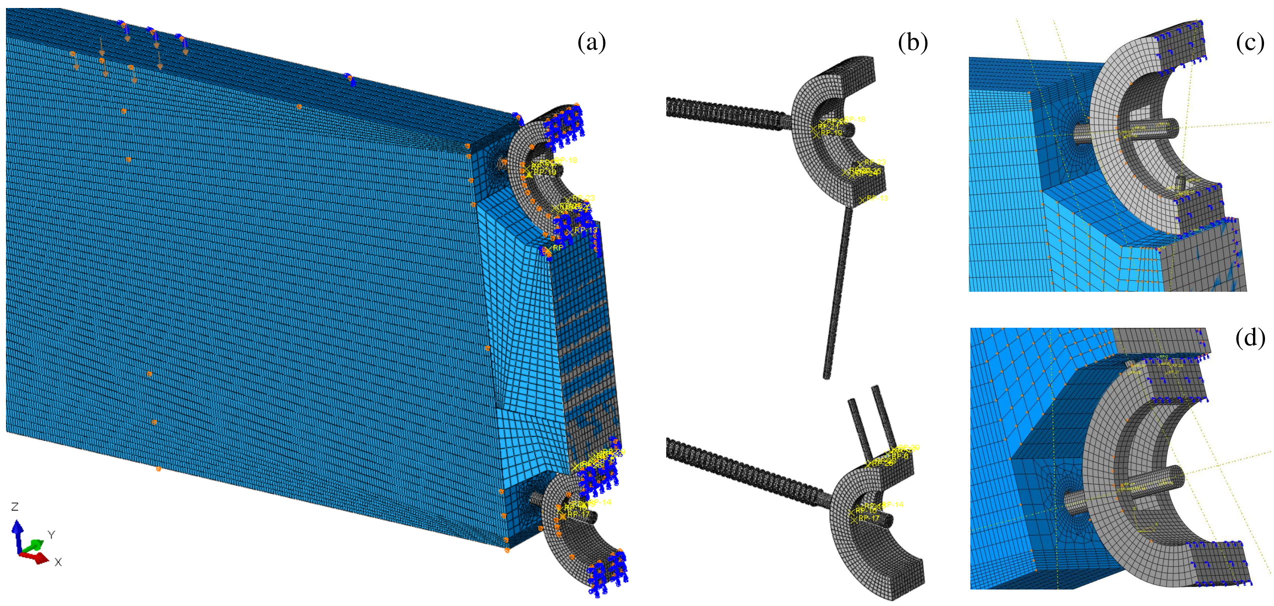

Figure 9: Visualisation of the numerical model: (a) detail at the splice joint, (b) steel parts of the joint, (c) detail at the compression coupler, (d) detail at the tension coupler.

Eight-node brick elements with reduced integration and hour-glass control (C3D8R) were used in the models. A sensitivity study was carried out in order to determine a satisfactory mesh size. The mesh was denser in the zones surrounding the rods.

The threaded rods and their interaction with timber were based on numerical models presented in [18, 26]. The effective length of the rods was 1200 mm, and the inner and the outer diameters of wood threads were 16.9 mm and 22.4 mm, respectively (see Figure 8). Contact properties between rods and timber utilised a "hard" contact behaviour in the normal direction and isotropic tangential behaviour with a coefficient of friction of 0.2, which was based on the study in [27]. The anchorage screws of the rod couplers (see Figure 9b) were modelled without threads (by the outer diameter) and with the interaction with the timber realised through a tie-constraint. This simplified approach was shown to be suitable for self-tapping screws in [28].

The relative slip between the rods and the couplers is rigidly constrained for all degrees of freedom, while the relative displacements between the couplers and the anchoring screws are prevented only in the vertical direction (along z-axis with reference to Figure 9).

The stiffness at the interface of two mutually compressed mating timber end faces is affected by end grain effects. These end grain effects are described in [18] by introducing a “crushing zone” in the vicinity of the timber end faces characterized by a crushing modulus, E_{cr}, and a crushing length, l_{cr}, The contact stiffness between the end timber faces in numerical models can thus be modelled by defining a linear elastic contact stiffness at the timber end face with a magnitude of E_{cr} / l_{cr}. Based on the experimental results in [18], the stiffness is here assumed as E_{cr} / l_{cr} = 914 MPa / 3 mm = 304 MPa/mm (see further description in the Appendix).

Material properties of wood are summarised in Table 2. Here, E is the modulus of elasticity, G is the shear modulus, ν is the Poisson’s ratio and σ_y represents the yield strength. The longitudinal direction (L) is the grain direction, and no distinction is made between tangential (T) and radial (R) directions.

Table 2: Material properties of wood used in numerical simulations

	[MPa]	[MPa]	[MPa]	[MPa]	[-]	[-]
Elastic	E_L (a)	E_R=E_T (a)	G_{LR}=G_{LT} (b)	G_{RT} (b)	ν_{LR}=ν_{LT} (b)	ν_{TR} (b)
	13000	400	600	30	0.6	0.315
Yield	σ_{yL} (b)	σ_{yR}=σ_{yT} (b)	σ_{yLR}=σ_{yLT} (b)	σ_{yRT} (b)		
	23	2.4	3	0.9		

(a) Manufacturer: Moelven industrier ASA, class L40 (GL30c)

(b) Estimations based on [29]

Hill’s yield surface [30] was applied to wood together with a linear isotropic hardening and associated flow rule. It should be noted that the material model gives no distinction between positive and negative stresses. No damage coupling was defined in order to describe brittle failure in tension and shear. However, as long as the post-elastic behaviour of the joint is governed by the plastic deformations of the steel parts and crushing of the compression zone of timber, the model provides a suitable description of the joint behaviour also in the non-linear domain. The uniaxial strength parameters were thus chosen to represent the compression stress states, and the hardening was formulated to fit the experimental results in [29] in compression parallel to the grain, such that plastic strains of 0.0035 correspond to the stress level of 33 MPa.

Steel was modelled as isotropic with E = 210 GPa and ν = 0.3. The plastic domain was described by von Mises’s yield criterion, linear isotropic hardening and associated flow rule. The yield strength and the hardening formulation of the threaded rods were based on the conducted tensile tests giving the following approximate values of plastic strains at the corresponding stress levels: 0 at 758 MPa and 0.031 at 925 MPa. Corresponding properties for structural steel S355 were used as 0 at 355 MPa and 0.25 at 510 MPa.

3. Results and discussion

3.1. Experimental results

Experimental results of bending tests of the splice connections are presented in terms of moment vs. rotation in the joint, see the plots in Figure 10.

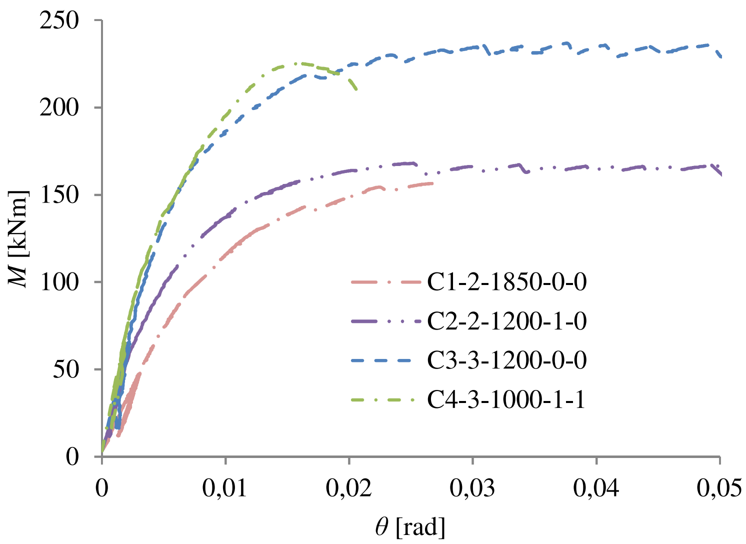

Figure 10: Moment-rotation curves based on data from digital image correlation monitored during bending tests.

The ultimate moment M_u and the elastic rotational stiffness k_θ are presented in Table 3. The splice efficiency with respect to moment capacity, η_M, is the ratio between the measured ultimate moment and the mean theoretical bending capacity of the unspliced timber cross-section. The efficiency with respect to rotational stiffness, η_k, relates the mid-span deflection of an unspliced beam (obtained with mean values of material characteristics) to that of a beam containing a splice connection.

Table 3: Experimental results of bending tests of splice connection

Notation	M_u		k_θ		Failure mode
	[kNm]	η_M [(a)]	[kNm/rad]	η_k [(b)]	
C1-2-1850-0-0	161/169	30 %	14863	52 %	Nut/Steel rods
C2-2-1200-1-0	173	30 %	24952	65 %	Steel rods
C3-3-1200-0-0	241	42 %	29167	68 %	Timber compression
C4-3-1000-1-1	230	40 %	35324	72 %	Rods withdrawal

input: GL30c: [(a)] $f_{m,mean}$ = 41.4 MPa [(b)] E_{mean} = 13000 MPa, G_{mean} = 650 MPa

The test of C1 initially failed in a brittle manner due to a nut-thread failure. However, the joint was reassembled and by use of two nuts at the tension side, the new test resulted in the ductile tensile failure of the threaded rods. The plot of C1 in Figure 10 represents the first test until the nut-thread failure. The rotational stiffness of C1 is low, compared to C2, which also had 2 rods per row. This is due to the use of standard M20 washers at the connection of the compression rods in the couplers, which did not provide sufficient support in order to prevent rotation of the rod-ends in the couplers. A considerably better rotational stiffness was achieved by the use of fitted internal washers in the compression couplers in the C2 configuration. It was, however, observed that even the use of internal fitted washers did not prevent the outward bending of the compression rods under increasing loading (see Figure 11e). The force transfer in the compression rods was thus limited, which in turn resulted in increased deformation of the timber in the compression zone. The failure was finally caused by a tensile rupture of the rods (see Figure 11d). As for C1, the standard M20 washers were also used in the C3 configuration. Insufficient rotational restraint of the compression rod-ends led to bending of the rods and increased utilisation of timber in compression (see Figure 11b and Figure 11c). Compression of timber is very ductile and the test was stopped after reaching large deformations without any significant decrease in capacity. The bending of the compression rods was prevented in the C4 configuration by anchoring the compression couplers and the use of internal fitted washers. However, shorter rods were used in C4 and the ultimate failure was caused by the withdrawal of the rods in tension. Note that no initial slips were observed in any of the performed tests.

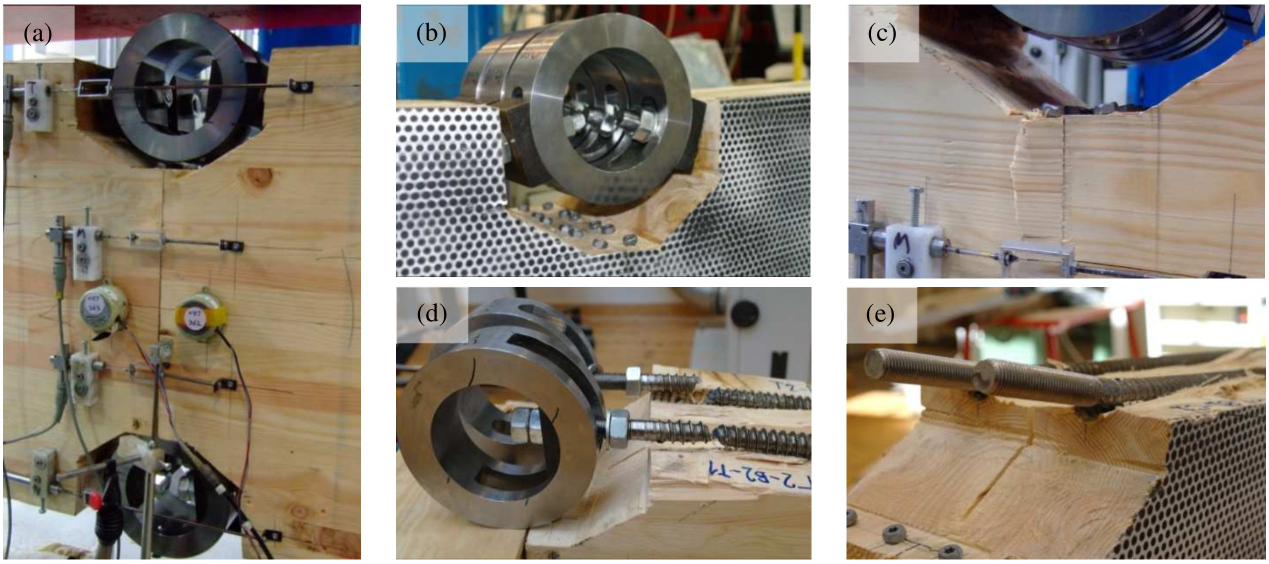

Figure 11: Joint details during and after tests: (a) C2 during test, (b) compression couplers of C3 after test, (c) failure at compression zone of C3, (d) tensile rupture of tension rods of C2, (e) compression rods of C2 after testing.

The experimental results demonstrate large rotational stiffness of the timber splice joints by the use of long threaded rods. In agreement with pure withdrawal tests of threaded rods [26], the relation between the effective length and the withdrawal stiffness is non-linear. This implies that increasing the effective length of the rods more than necessary in order to obtain the steel failure has a negligible effect on the withdrawal stiffness. Tensile ruptures of the rods were encountered for rods of 1200 mm effective length in the current investigation. In order to fully utilise the large withdrawal stiffness of the rods, slips between the rods and the couplers should be minimised. In addition, bending of the compression rods can be avoided by anchoring the couplers to the timber.

3.2. Analytical prediction of capacity and stiffness compared to experimental and numerical results

The moment capacity M_u and the rotational stiffness k_θ of the joint obtained from experiments, numerical models and the proposed analytical model are summarised in Table 4.

Two sets of results are shown for the analytical model. The first set, denoted as Anal.A, was obtained by the use of the withdrawal stiffness of the threaded rods, K_w, obtained from numerical models. In the second set, Anal.B, K_w was obtained by the model proposed in [26] with the assumption of the so-called pull-shear boundary conditions. While the set of results Anal.A gives a good agreement between the analytical and the experimental results in terms of rotational stiffness, the set of results Anal.B gives conservative estimates of the rotational stiffness of the joint.

The rotational stiffness predicted by the numerical models was in a good agreement with the experimental results.

Table 4: Experimental, numerical and analytical results

n_r	k_θ [kNm/rad]				M_u [kNm]		
	Exp.	Anal.A	Anal.B	Num.	Exp.	Anal.A	Num.
2	24952 (C2)	23227	18780	23755	169/173	188	190
3	35324 (C4)	34044	27513	36522	241/230*	284/243*	286

Input geom.: b = 215 mm, h_t = 325 mm, a_i = 415 mm for lower and -90 mm for upper rods, d = 22.4 mm, d_1 = 16.9 mm, l_f = 45 mm, *l_{ef} = 1000 mm, otherwise l_{ef} = 1200 mm

Material characteristics used as an input to the analytical models (mean values):

K_w	243 kN/mm in Anal.A	Withdrawal stiffness of threaded rods obtained by numerical model
K_w	176 kN/mm in Anal.B	Withdrawal stiffness of threaded rods obtained by model in [26]
E	13 000 MPa	MOE of timber parallel to the grain (see Table 2)
E_s	210 GPa	MOE of steel
E_{cr}	914 MPa	Crushing modulus [18] (see Appendix)
l_{cr}	3 mm	Crushing length [18] (see Appendix)
k_t	710 MPa	Foundation modulus of timber transverse to the grain [31, 32] (see Appendix)
k_l	1300 MPa	Foundation modulus of timber longitudinal to the grain [31, 32] (see Appendix)
K_{co}	450 kN/mm	Stiffness of the rod coupler obtained by numerical model (see Appendix)
R_u	207.6 kN	Tensile capacity of the threaded rods obtained by tensile tests (see 2.2.2)
R_{ax}	Var. for var. rod lengths	Withdrawal strength of the threaded rods under pure axial loading by model in [33]

The experimentally obtained ultimate moments were affected by bending of the compression rods in the configurations C1, C2 and C3 due to insufficient stiffness between the rods and the couplers, while the withdrawal of the tension rods limited the capacity in the C4 configuration. The analytical and numerical models assume no slip between the rods and the couplers, and the predicted moment capacity is, therefore, higher compared to the experimental results. A good mutual agreement is obtained for the moment capacity predicted by the analytical and the numerical models. The ultimate load in the numerical model was governed by a combination of a full utilization of the capacity of the rods in tension and bending of the compression rods together with a "plastification" of the timber compression zone. Note that the numerical models were not formulated to predict the withdrawal failure of the rods, which was the failure mode in the C4 configuration. The moment capacity predicted by the numerical and the analytical models can thus be interpreted as a maximum moment capacity of the joint, assuring that the outward bending of the compression rods is prevented.

The moment-rotation curves obtained by the numerical simulations are presented together with the experimental results (for configurations containing the internal fitted washers) in Figure 12. The numerical simulations were performed both with the compression rod couplers anchored to the timber, i.e. in correspondence with the results in Table 4 (curves denoted as num.Alt.I) and without anchoring the compression couplers (curves denoted as num.Alt.II). The numerical results show that, by anchoring the compression couplers, the moment capacity is increased by 5 %, while the anchorage has a negligible effect on the rotational stiffness of the joint. When comparing the numerical and the experimental results in the case of 2 rods per row, it is observed that the moment capacity of the joint can be enhanced by 5 % if the slip between the rods and the couplers is entirely prevented and by an additional 5 % by anchoring the couplers. In the case of 3 rods per row, the couplers were anchored in the experimental setup (C4) and the failure was caused by the withdrawal of the tension rods. It is seen that by providing a sufficient effective length of the rods, an increase in moment capacity by 24 % can be achieved. With reference to Table 3, the joint efficiency, in terms of capacity, is thus improved from 40 % to 50 % in the configuration with 3 rods per row.

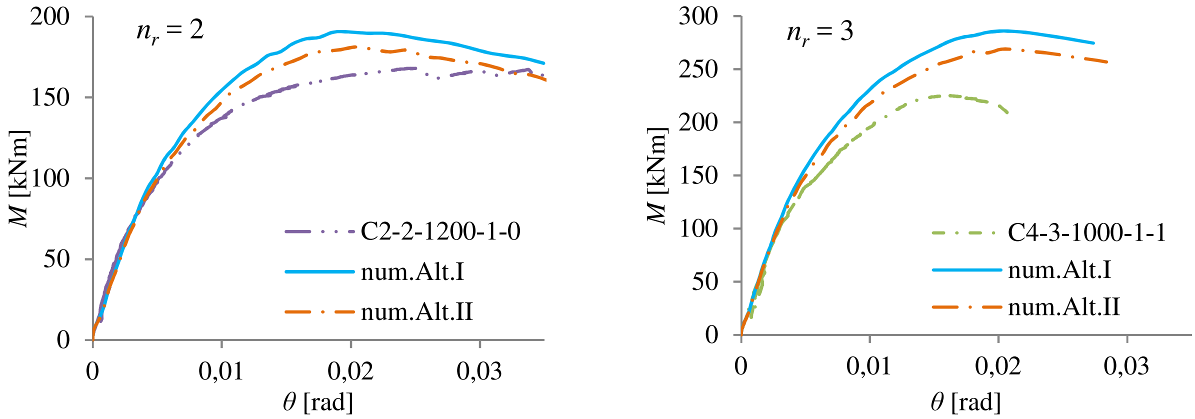

Figure 12: Moment-rotation curves obtained by the numerical models compared to the experimental results.

As discussed in Section 2.2, the rod couplers used in the current investigation were generally-suited prototypes not optimised for the particular joint layout. A further optimisation of the design will probably allow a reduction of the size of the couplers, leading to smaller openings in the timber beams. If the height of the openings is reduced from the current 130 mm to 80 mm, the analytical model shows an increase of the rotational stiffness and the moment capacity by 7 % and 1%, respectively.

3.3. Combined action of bending moment and normal force

The capacity under the combined action of bending moment and normal force was studied by use of numerical models for the configuration of 2 rods per row. The results of the analyses together with the analytical solutions are shown in Figure 13 by the interaction diagrams of bending moment *M* and normal force *N*. In this study, two sets of analyses by numerical models were performed. In the first set, the rod couplers were anchored to the timber members both at the tension and the compression side (results denoted as Num.Anch.). In the second set, no interaction between the couplers and the timber was applied (results denoted as Num.Unanch.). The analytical solution was obtained by the use of Eq. (7). In the case of the "anchored" set of analyses, N_u and M_u were obtained by Eqs. (8) and (3), respectively. If the rod couplers are not anchored to the timber, the rods can be bended and the force transfer through the rods is limited. The analytical solution shown in Figure 13 for the case of "unanchored" couplers was thus obtained for N_u determined by Eq. (8), disregarding the contribution from the rods, but assuming the maximum compression strength of timber $f_{c,0}$. M_u was obtained by the use of Eq. (3) with disregard of the compression rods. The input parameters to the analytical models are summarised in Section 3.2 (K_w from numerical models was used herein).

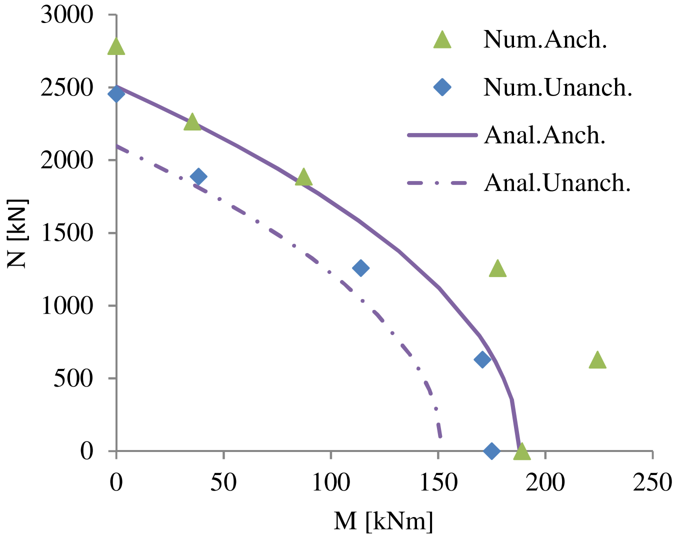

Figure 13: Interaction M-N diagram for joint with 2 rods per row.

The ultimate load modes in the numerical models differ in dependence on the ratio of M/N. For higher ratios of M/N, the ultimate load is governed by a full utilisation of the axial capacity of the rods in tension. For lower ratios of M/N, the ultimate load is governed by bending of the rod in compression together with full utilization of timber in compression. It should be noted that the numerical models were not formulated to predict the brittle failures in timber in direction perpendicular to the grain and the shear failures. Therefore, the obtained results should be interpreted with caution since they likely represent an upper bound. Nevertheless, Figure 13 indicates that the proposed simple analytical interaction model enables a reasonable prediction of the joint capacity under combined action of bending moment and normal force.

4. Concluding remarks

The present investigation shows that splicing of massive glulam sections can effectively be achieved by use of inclined long threaded rods. The experimentally investigated prototype joint featured large rotational stiffness without any initial slip. It was shown that the boundary conditions at the rod-ends affect both the rotational stiffness and the moment capacity considerably. The reported joint moment capacity appear to be sufficient for the intended joint application in timber network arch bridges, for which the design is governed by a normal force [4]. In addition, the location of the joint can be optimized with respect to extreme values of bending moments in the arch.

For practical joint design, analytical relations validated by experiments and numerical models are proposed for the determination of the rotational stiffness and moment capacity. In addition, a simple model for predicting the capacity under combined action of bending moment and normal force is proposed and compared to the results obtained by numerical models. Note that the formulation of the numerical models did not allow capturing all failure modes. Therefore, care should be taken when interpreting the numerical results.

The rod inclination to grain prevents the loss of capacity in case of shrinkage cracks in close proximity to the threaded rods. In the current investigation, the rod-to-grain angle was 5 degrees, which is considered appropriate in order to bridge possible shrinkage cracks, as well as to maintain the large withdrawal stiffness and capacity of the rods. By providing sufficient effective length, the failure mode is ductile, due to yielding of the rods. As shown in [34], under the combined action of axial and lateral loads, both the capacity and the initial stiffness of the threaded rods are reduced for both increased rod-to-grain and load-to-rod angles.

In timber network arch bridges, the bending moment acting in the joint will change orientations for different traffic load positions and different directions of wind loads. In addition, a considerable normal force will act in the connection, transmitted through both the contact of the timber end faces and the rods. Hence, the layout of the connection must be symmetric (i.e. the rod detailing at both sides of the connection must allow the transfer of both tension and compression) and the timber end faces must be in mutual contact provided by tightening of the rods during assembly. It should be noted that the scope of the present work did not cover the fatigue resistance. Yet, the preliminary results of fatigue tests of axially loaded threaded rods indicate that the fatigue resistance of timber is large compared to steel, and the fatigue capacity of joints with this type of connector is thus governed by the resistance of the steel components [35, 36].

The proposed splicing technique utilises long threaded rods embedded with a small inclination to the grain. The hygroscopic deformations in timber normal grain are thus not restrained, resulting in a favourable solution regarding the moisture induced stresses in the joint. However, self-tapping screws embedded perpendicular to the grain were used to reinforce the joint and to anchor the couplers to the timber, which may initiate moisture induced cracks [37, 38]. The self-tapping screws used in the current investigation were not optimised and further investigations should be carried out to eliminate the possible effect on the development of the moisture induced cracks.

Acknowledgment

This work was funded by the WoodWisdom-Net+ project DuraTB ("Durable Timber Bridges") and the support from the funding bodies and partners is gratefully acknowledged. The authors would also like to acknowledge Hallvard Oltedal Veium for his important contributions and experimental work.

Appendix

Input parameters to the expressions presented in Sections 2.1.1 and 2.1.2

The equivalent length of the timber compression (crushing) zone at each side of the contact interface, l_c, is given by [18]:

$$l_c = 0.85 \cdot h_t + l_{cr} \cdot \frac{E}{E_{cr}} \tag{9}$$

where h_t is the height of timber end faces in mutual contact (see Figure 3), and E_{cr} and l_{cr} are the crushing modulus and the crushing length, respectively.

The first term in Eq. (9) characterizes the compliance of the wood in compression and approximately defines a local area, in close proximity to the splice joint, for which the Navier's hypothesis is violated and where the stress state is a combination of compression stresses parallel to the grain, tensile stresses perpendicular to the grain and shear stresses. The second term characterizes the deformation at the end grains of two mutually compressed mating timber end faces and it is derived by introducing a crushing zone characterized by a crushing modulus, E_{cr}, and a crushing length, l_{cr}. The parameters of the crushing zone were obtained experimentally. Based on the experimental results performed for glulam class GL30c, it is suggested in [18] to use l_{cr} = 3 mm with the corresponding E_{cr} = 914 MPa, yielding the stiffness of the crushing zone $E_{cr} / l_{cr} \cong 300\ \mathrm{N/mm^3}$.

The stiffness of the i-th rod row, K_{si}, given by Eq. (10), is obtained as a system of three springs in series representing: 1) the stiffnesses of the threaded rods in the direction of the applied force at each side of the connection denoted as K_p, and, 2) the stiffness of the rod coupler denoted as K_{co}. The number of steel rods in one row equals n_r.

$$K_{si} = n_r \cdot \frac{K_p \cdot K_{co}}{2 \cdot K_{co} + K_p} \tag{10}$$

The stiffness of the threaded rods in the direction of the applied force (parallel to the grain), K_p, is affected by the rod-to-grain and load-to-rod angles, and by the boundary conditions at the rod-end. These effects were studied and analytical relations for the stiffness prediction were derived in [34]. In the following, the relations associated with the actual geometrical layout are presented.

The rod stiffness in the direction of the applied force K_p is found as the interaction of the axial rod stiffness K_{ax} and the lateral rod stiffness K_v at the rod-end by [34]:

$$K_p = \frac{K_{ax} \cdot K_v}{K_{ax} \cdot \sin^2(\gamma) + K_v \cdot \cos^2(\gamma)} \tag{11}$$

If the displacements transverse to the load direction are prevented (by anchoring the coupler to the timber), the rod stiffness is determined by [34]:

$$K_p = K_{ax} \cdot \cos^2(\gamma) + K_v \cdot \sin^2(\gamma) \tag{12}$$

The stiffness in the axial direction K_{ax} of the rod is found by [34]:

$$K_{ax} = \frac{K_w \cdot K_{ax,f}}{K_w + K_{ax,f}} \tag{13}$$

where K_w is the withdrawal axial stiffness of the threaded rod. The axial stiffness of the free part of the rod not embedded in timber is determined as $K_{ax,f} = E_s \cdot A_s / l_f$, where l_f is the length of the free part of the rod between the timber member and the rod fastening in the coupler, E_s is the elastic modulus of steel and A_s is the cross-sectional area of the rods determined with the core diameter of the rods d_1.

Under the assumption of a rotational restraint at the rod-end implied by a connection in the couplers, the lateral stiffness at the rod-end, K_v, is found by [34]:

$$K_v = \frac{12kEI\left(4EI\lambda^3 + kl_f\right)}{48\left(EI\right)^2\lambda^4 + 8kEI\lambda l_f\left(2l_f^2\lambda^2 + 3l_f\lambda + 3\right) + k^2 l_f^4} \tag{14}$$

where EI is the flexural stiffness of the rods obtained as $EI = E_s \cdot \pi \cdot d_1^4 / 64$, the parameter λ is found as $\lambda = \sqrt[4]{k/(4EI)}$ and k is the foundation modulus of timber obtained by the interaction of foundation moduli of timber longitudinal to the grain, k_l, and transverse to the grain, k_t, as [34]:

$$k = \frac{k_l \cdot k_t}{k_l \cdot \cos^2(\gamma) + k_t \cdot \sin^2(\gamma)} \tag{15}$$

The withdrawal strength of the rods is reduced compared to pure axial loading due to the inclination of the rods and the imposed rotational restraint at the rod-end (the rods are loaded by a combination of a lateral force and a bending moment). Similar to the model proposed in [18], the ultimate withdrawal strength of the rods R_{axu} is found by a linear reduction of the effective length of the threaded rods:

$$R_{axu} = R_{ax} \cdot \left(\frac{l_{ef} - l_x}{l_{ef}} \right) \qquad (16)$$

where R_{ax} is the withdrawal strength of the threaded rods under pure axial loading (R_{ax} can be determined for the effective length of the threaded rods, l_{ef}, by the use of the model proposed in [33] with the assumption of the so-called pull-shear boundary conditions), and l_x is a free length of the rod that is not considered to contribute to the withdrawal capacity.

The free length of the rod, l_x, can be determined in the same manner as in [18] by assuming an interaction of lateral force and bending moment and respecting the actual boundary conditions at the rod-end. However, the exact analytical solution becomes unhandy to use and the following conservative simplification is thus proposed:

$$l_x = \pi \cdot d_1 \cdot \sqrt[4]{\frac{\pi \cdot E_s}{k}} \qquad (17)$$

References

[1] K. Bell, Structural systems for glulam arch bridges, International Conference on Timber Bridges (ICTB 2010), Lillehammer, Norway, 2010.

[2] K.A. Malo, A. Ostrycharczyk, R. Barli, I. Hakvåg, On development of network arch bridges in timber, International Conference on Timber Bridges (ICTB 2013), Las Vegas, USA, 2013.

[3] K. Bell, L. Wollebæk, Large, mechanically joined glulam arches, Proceedings of the World Conference on Timber Engineering (WCTE 2004), Lahti, Finland, 2004.

[4] M. Cepelka, K.A. Malo, Effect of on-site splice joints for timber network arch bridges, International Conference on Timber Bridges (ICTB 2017) Skellefteå, 2017.

[5] L. Wollebæk, K. Bell, Stability of glulam arches, Proceedings of the World Conference on Timber Engineering (WCTE 2004), Lahti, Finland, 2004.

[6] J. Veie, M. Østgårdstrøen, Steibrua, Norwegian Public Roads Administration, Brukonferansen 2016 - available at https://www.vegvesen.no/_attachment/1606923/binary/1145671?fast_title=Steibrua.pdf, (last accessed 06/2017).

[7] M. Cepelka, Splicing of Large Glued Laminated Timber Elements by Use of Long Threaded Rods, vol Dissertation, Norwegian University of Science and Technology, NTNU, 2017.

[8] N. Gattesco, A. Gubana, M. Buttazzi, M. Melotto, Experimental investigation on the behavior of glued-in rod joints in timber beams subjected to monotonic and cyclic loading, Engineering Structures 147 (2017) 372-384, https://doi.org/10.1016/j.engstruct.2017.03.078.

[9] J. Ogrizovic, F. Wanninger, A. Frangi, Experimental and analytical analysis of moment-resisting connections with glued-in rods, Engineering Structures 145 (2017) 322-332, http://dx.doi.org/10.1016/j.engstruct.2017.05.029.

[10] B.H. Xu, A. Bouchaïr, P. Racher, Analytical study and finite element modelling of timber connections with glued-in rods in bending, Construction and Building Materials 34 (2012) 337-345, http://dx.doi.org/10.1016/j.conbuildmat.2012.02.087.

[11] H. Yang, W. Liu, X. Ren, A component method for moment-resistant glulam beam–column connections with glued-in steel rods, Engineering Structures 115 (2016) 42-54, https://doi.org/10.1016/j.engstruct.2016.02.024.

[12] G. Tlustochowicz, E. Serrano, R. Steiger, State-of-the-art review on timber connections with glued-in steel rods, Materials and Structures 44 (2011) 997-1020, https://doi.org/10.1617/s11527-010-9682-9.

[13] N. Gattesco, A. Gubana, M. Buttazi, Cyclic behaviour of glued-in joints under bending moments, Proceedings of the World Conference on Timber Engineering (WCTE 2010), June 20-24, Riva Del Garda, Trento, Italy, 2010.

[14] E. Gehri, High Performing Jointing Technique Using Glued-in Rods, Proceedings of the World Conference on Timber Engineering (WCTE 2010), June 20-24, Riva Del Garda, Trento, Italy, 2010.

[15] R. Steiger, E. Gehri, R. Widmann, Pull-out strength of axially loaded steel rods bonded in glulam parallel to the grain, Materials and Structures 40 (2007) 69-78, https://doi.org/10.1617/s11527-006-9111-2.

[16] Y. Wakashima, K. Okura, K. Kyotani, Development of ductile semi-rigid joints with lagscrewbolts and glued-in rods, Proceedings of the World Conference on Timber Engineering (WCTE 2010), June 20-24, Riva Del Garda, Trento, Italy, 2010.

[17] G. Parida, H. Johnsson, M. Fragiacomo, Provisions for Ductile Behavior of Timber-to-Steel Connections with Multiple Glued-In Rods, Journal of Structural Engineering 139 (2013) 1468-1477, https://doi:10.1061/(ASCE)ST.1943-541X.0000735.

[18] M. Cepelka, K.A. Malo, Moment resisting splice of timber beams using long threaded rods and grout-filled couplers – Experimental results and predictive models, Construction and Building Materials 155 (2017) 560-570, https://doi.org/10.1016/j.conbuildmat.2017.08.089.

[19] CEN, EN 1995-1-1:2004: Design of timber structures. Part 1-1: General-Common rules and rules for buildings, European committee for standarization, Brussels, 2004.

[20] H.J. Larsen, Design of Structures Based on Glulam, LVL an Other Solid Timber Products, in: S. Thelandersson, H.J. Larsen (Eds.), Timber Engineering, Wiley, 2003.

[21] H.J. Blass, Traglastberechnung von Drückstäben aus Brettschichtholz (Load-bearing capacity of compression members of glued laminated timber), Bauingeniør (1988) 245-251.

[22] GOM Optical Measuring Techniques, ARAMIS, User Manual-Software, 2009.

[23] CEN, EN 26891:1991 (ISO 6891:1983) Timber structures, Joints made with mechanical fasteners, General principles for the determination of strength and deformation characteristics 1991.

[24] CEN, EN 14080:2013: Timber structures-Glued laminated timber and glued solid timber - Requirements, European Committee for Standardization, 2013.

[25] D.S.S.C. DSS, Abaqus analysis user's guide, Version 6.14, 2014.

[26] H. Stamatopoulos, K.A. Malo, Withdrawal stiffness of threaded rods embedded in timber elements, Construction and Building Materials 116 (2016) 263-272, http://dx.doi.org/10.1016/j.conbuildmat.2016.04.144.

[27] R. Koubek, K. Dedicova, Friction of wood on steel. Master Thesis, vol Master thesis, Linnaeus University, 2014.

[28] M. Oudjene, V.-D. Tran, E.-M. Meghlat, H. Ait-Aider, Numerical models for self-tapping screws as reinforcement of timber structures and joints, in: W.W. J. Eberhardsteiner, A. Fadai, M. Pöll (Ed.)

Proceedings of the World Conference on Timber Engineering (WCTE 2016), August 22-25, 2016, Vienna University of Technology, Austria, ISBN: 978-3-903039-00-1, Vienna, Austria, 2016.

[29] K.B. Dahl, Mechanical properties of clear wood from Norway spruce. Dissertation, Department of Structural Engineering, vol Doctoral thesis, Norwegian University of Science and Technology, 2009.

[30] R. Hill, A Theory of the Yielding and Plastic Flow of Anisotropic Metals, Proceedings of the Royal Society of London 193 (1948) 281-297.

[31] N. Gattesco, Strength and local deformability of wood beneath bolted connectors, Journal of Structural Engineering 124 (1998) 195-202.

[32] N. Gattesco, I. Toffolo, Experimental study on multiple-bolt steel-to-timber tension joints, Materials and Structures/Materiaux et Constructions 37 (2004) 129-138.

[33] H. Stamatopoulos, K.A. Malo, Withdrawal capacity of threaded rods embedded in timber elements, Construction and Building Materials 94 (2015) 387-397, http://dx.doi.org/10.1016/j.conbuildmat.2015.07.067.

[34] M. Cepelka, K.A. Malo, H. Stamatopoulos, Effect of rod-to-grain angle on capacity and stiffness of axially and laterally loaded long threaded rods in timber joints, European journal of Wood and Wood Products (in press) (2018).

[35] K.A. Malo, A. Pousette, S. Thelandersson, S. Fortino, L. Salokangas, J. Wacker, Durable timber bridges Final report and guidelines, RISE Research Institutes of Sweden, 2017.

[36] H. Stamatopoulos, K.A. Malo, Fatigue strength of axially loaded threaded rods embedded in glulam at 45º to the grain, International Conference on Timber Bridges (ICTB2017), Skellefteå, Sweden, 2017.

[37] V. Angst, K.A. Malo, Effect of self-tapping screws on moisture induced stresses in glulam, Engineering Structures 45 (2012) 299-306, http://dx.doi.org/10.1016/j.engstruct.2012.06.048.

[38] P. Dietsch, Effect of reinforcement on shrinkage stresses in timber members, Construction and Building Materials 150 (2017) 903-915, http://dx.doi.org/10.1016/j.conbuildmat.2017.06.033.